Semiclassical wave functions for open quantum billiards

Fabian Lackner,[*] Iva Březinová,[†] and Joachim Burgdörfer
Institute for Theoretical Physics, Vienna University of Technology, Wiedner Hauptstraße 8-10/136, 1040 Vienna, Austria, EU

Florian Libisch
Department of Mechanical and Aerospace Engineering, Princeton University, New Jersey, USA
(Received 15 March 2013; published 19 August 2013)

We present a semiclassical approximation to the scattering wave function $\Psi(\mathbf{r},k)$ for an open quantum billiard, which is based on the reconstruction of the Feynman path integral. We demonstrate its remarkable numerical accuracy for the open rectangular billiard and show that the convergence of the semiclassical wave function to the full quantum state is controlled by the mean path length or equivalently the dwell time for a given scattering state. In the numerical implementation a cutoff length in the maximum path length or, equivalently, a maximum dwell time $\tau_{\max}$ included implies a finite energy resolution $\Delta E \sim \tau_{\max}^{-1}$. Possible applications include leaky billiards and systems with decoherence present.

DOI: 10.1103/PhysRevE.88.022916 PACS number(s): 05.45.Mt, 03.65.Sq, 03.65.Nk, 73.22.Dj

I. INTRODUCTION

In his doctoral thesis R. P. Feynman, extending earlier work by Dirac [1], developed a novel formulation of quantum mechanics [2]. Unlike Schrödinger's formulation in terms of the solution of a partial differential equation Feynman based his description on the intuitive picture of paths connecting two points in space. Each path carries an amplitude and a phase that is given by its classical action. Incorporating the principle of superposition, the propagator, i.e., the probability amplitude to move from one point in space to another, is given by the sum (i.e., integral) over all paths connecting these points. While this path integral formulation is equivalent to the standard Schrödinger theory, its implementation as an operational algorithm to solve quantum problems is complicated due to the mathematical difficulties associated with the path integration. One of its advantages is, however, the conceptual insight it can provide. Most importantly, modern semiclassical theory invokes the convergence of the path manifold as contained in Feynman's path integral towards a discrete subset of classical paths of extremal action as $\hbar \to 0$.

The semiclassical approximation applicable at the border between quantum and classical mechanics follows from the path integral formalism in the limit that the variation of the classical action is large compared to $\hbar$ for small path variations. Mesoscopic systems with linear dimension D large compared to the de Broglie wavelength λ_{dB}, $\lambda_{\mathrm{dB}} \ll D$, represent prototypical cases for which semiclassical approximations are frequently invoked since in many cases *ab initio* quantum calculations become unfeasible. Moreover, the description in terms of paths can provide detailed physical insights into spectral and transport properties. For example, dephasing and decohering interactions are associated with a characteristic mean free path length ℓ_{MFP}, thereby limiting phase coherent transport to short paths, $\ell < \ell_{\mathrm{MFP}}$. A well known example is the open quantum billiard in the ballistic regime, which has been extensively studied in the last several years both experimentally and theoretically (see, e.g., Refs. [3–5] and references therein). The semiclassical approximation has contributed to the understanding of phase coherent transport effects such as conductance fluctuations and weak localization [6–26]. Most semiclassical approximations to date have focused on either the spectral density $\rho(E)$ [27] or transport coefficients determined for ballistic transport by S matrix elements [10,28]. Semiclassical calculations of the wave function $\Psi(\mathbf{r},k)$ itself which test the quantum to classical transition locally on the finest scale have remained a challenge. Few pioneering studies have been performed: scars in closed billiards could be reproduced by semiclassical calculations of the energy-averaged probability density $\langle|\Psi(\mathbf{r},k)|^2\rangle$ [29]. For open chaotic billiards, statistical properties of the wave functions such as nodal point distributions have been found in good agreement with random wave models [30]. In the regime of high incident energies with a large number of open modes, quantum calculations [31] for the open chaotic stadium billiard have shown that the wave function closely mirrors the path bundles [12] of short classical scattering trajectories. A simple semiclassical approximation to the wave function yields good qualitative agreement with the quantum wave function.

We present in the following an accurate semiclassical determination of the fine-scale wave function $\Psi(\mathbf{r},k)$ for an open ballistic billiard. We construct the wave function in terms of a sum over paths connecting the entrance lead with an arbitrary point $\mathbf{r}$ in the interior of the billiard closely following the Feynman path integral prescription. We employ the pseudopath semiclassical approximation (PSCA) [14–17] to include both classical and diffractive, i.e., nonclassical paths into the path sum. We aim at a quantitative agreement with quantum wave functions for the low-energy regime with only few open modes in the leads (quantum wires) and a semiclassical description that pertains to the interior of the billiard. We gauge the accuracy of the wave function by comparison with full quantum wave functions. For technical reasons, we focus on the rectangular billiard for which the enumeration and summation of paths is still feasible since it is a prototypical example of a integrable system. We show that the convergence towards the quantum wave function is

[*]fabian.lackner@tuwien.ac.at
[†]iva.brezinova@tuwien.ac.at

controlled by the dwell time or, equivalently, by the mean path length of the scattering state at given energy.

The outline of the paper is as follows. In Sec. II we briefly review the PSCA of the constant energy propagator and present its extension to calculations of wave functions of open quantum billiards. Concurrent calculations of the full quantum scattering state as well as its truncated form in which Fourier components associated with long path length are filtered out are discussed in Sec. III. In Sec. IV we present a quantitative comparison between semiclassical and quantum wave functions. We relate the convergence of the semiclassical wave function towards the exact quantum wave function to the dwell time, or, equivalently, to the Eisenbud-Wigner-Smith (EWS) delay time of the scattered wave inside the ballistic cavity. In the outlook (Sec. V) we briefly discuss future applications to leaky billiards and decoherence processes where long (coherent) paths or delay times are effectively suppressed and the PSCA offers a simple route to construct wave functions when short paths dominate the dynamics.

II. SEMICLASSICAL THEORY FOR SCATTERING STATES

A. Rectangular ballistic billiard

We discuss in the following the PSCA for wave functions with the help of the specific example of a squared (rectangular) open billiard [Fig. 1(a)]. The lead width $d = 1/16$ is small compared to the linear dimension $D = 1$ in reduced units. Consequently, the short-wave limit $\lambda_{\mathrm{dB}} \ll D$ is reached for the internal dynamics of the cavity while the motion inside the leads (or quantum point contacts) is still in the quantum regime for low transverse mode numbers n with transverse wave number $k_{y,n} = n\pi/d$. The longitudinal wave number is $k_{x,n} = \sqrt{k^2 - k_{y,n}^2}$. All wave numbers are given in the following in units of π/d. The PSCA is designed to describe the semiclassical dynamics for billiards which are coupled to quantum wires. The asymptotic scattering boundary condition

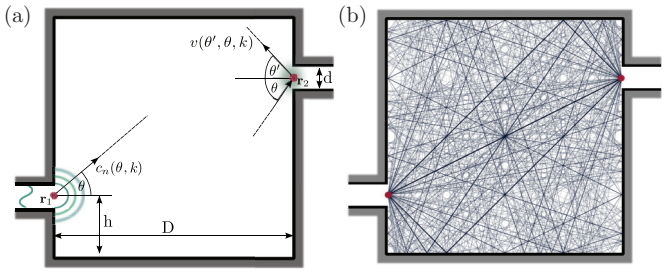

FIG. 1. (Color online) (a) Geometry of the rectangular (square) billiard with side length $D = 1$ and equal lead widths $d = 1/16$. The placement of the leads is point symmetric with offset $h = 0.25$. The diffractive couplings from the leads (quantum point contacts) to the cavity, $c_n(\theta,k)$, and for backscattering into the cavity $v(\theta',\theta,k)$ are sketched. The quantum point contacts (red dots) placed in the center of the leads are located at the coordinates $(x_1 = 0, y_1 = 0)$ and $(x_2 = D, y_2 = D - 2h)$. (b) The set of classical paths that connect the two quantum point contacts up to the maximal length $L = 10$. The color intensity of the paths is proportional to their deflection factor defined in Eq. (2).

is defined by the incoming wave

$$\Psi_{n,k}(\mathbf{r}) = \frac{1}{\sqrt{k_{x,n}}}\chi_n(y)e^{ik_{x,n}x}, \tag{1}$$

where (x,y) are the local coordinates along and perpendicular to the entrance lead and $\chi_n(y) = \sqrt{\frac{2}{d}}\sin[\frac{n\pi}{d}(y - \frac{d}{2})]$ is the transverse wave function of mode n. $\Psi_{n,k}(\mathbf{r})$ is flux normalized. The center of our coordinate system is the quantum point contact at the entrance lead denoted by $\mathbf{r_1} = (x = 0, y = 0)$ (see Fig. 1). The energy of the scattering state is given by $E = k^2/2$. The potential in the interior of the billiard cavity vanishes, $V = 0$, and is infinitely high at the walls. Dephasing and decohering interactions with the environment are not included in V. We comment on the influence of decohering processes on the path length distribution below.

The classical dynamics of transport from the entrance to the exit lead (transmission) or back to the entrance (reflection) is given by all classical paths p connecting the quantum point contacts (located at the center of the lead junctions) with each other. The action of a classical path p with path length L_p is given by $S_p = kL_p$. The classical phase space is structured in paths (or path bundles [12] when the finite size of the lead openings is taken into account) whose weight (area in phase space) is given by the deflection factor

$$D_p(k) = \left| \begin{matrix} \frac{\partial^2 S}{\partial \mathbf{r}'\partial \mathbf{r}}, \frac{1}{k}\frac{\partial^2 S}{\partial \mathbf{r}\partial k} \\ \frac{1}{k}\frac{\partial^2 S}{\partial \mathbf{r}'\partial k}, \frac{1}{k^2}\frac{\partial^2 S}{\partial k^2} \end{matrix} \right|. \tag{2}$$

In Fig. 1(b) we depict several classical paths connecting the entrance and exit point contact. Each path represents a path bundle and its color intensity is proportional to its weight, i.e., the deflection factor. For the rectangular billiard the deflection factor is exactly $D_p = 1/(kL_p)$. It is strictly positive and free of singularities. Consequently, the Maslov index μ_p entering semiclassics is given by

$$\mu_p = 2N_p, \tag{3}$$

where N_p is the number of reflections from the hard wall along path p. Note that one could alternatively incorporate von Neumann boundary conditions by setting the Maslov index equal to zero.

B. PSCA for scattering states

Starting point for the development of a semiclassical approximation to the wave function of the scattering state in the interior of the billiard is its expression in terms of the Green's function $G(\mathbf{r}',\mathbf{r},k)$,

$$\Psi_n(\mathbf{r}',k) = -i\sqrt{k_{x,n}}\int_{-d/2}^{d/2} G(\mathbf{r}',x = 0,y)\chi_n(y)dy, \tag{4}$$

for an incoming particle with wave number $k = \sqrt{2E}$ in mode n. The scattering boundary condition [Eq. (1)] at the lead entrance $(x = 0, y)$ acts as a source and the Green's function or constant-energy Feynman propagator connects the entrance point with the observation point via all (nonclassical) paths. Eq. (4) contains an integral over all entrance points with transverse coordinate y.

We note that the Fisher-Lee equation [32] expressing the S-matrix elements in terms of G is a special case of Eq. (4).

For example, the transmission amplitude t_{mn} is given by

$$t_{mn}(k) = -i\sqrt{k_{x,m}k_{x,n}} \times \iint \chi_m^*(y')G(x'=D,y',x=0,y;k)\chi_n(y)dy'dy, \tag{5}$$

where the integral over y' extends over all coordinates at the exit lead weighted with the outgoing mode amplitude $\chi_m(y')$ in the exit channel. The transmission (reflection) matrix is related to the S matrix as $t_{mn} = S^{2,1}_{mn}$ and $r_{mn} = S^{1,1}_{mn}$. The conductance g of the quantum billiard is determined by the Landauer formula [33,34]

$$g(k) = \frac{2e^2}{h}T(k) = \frac{2e^2}{h}\sum_{n=1}^{N}\sum_{m=1}^{N}|t_{mn}(k)|^2, \tag{6}$$

where N is the number of open modes in the leads (in our case the leads have equal width).

The semiclassical approximation to Eqs. (4) and (5) involves two steps: First, the evaluation of the integrals over the entrance and exit leads by either a stationary phase approximation (SPA) as done in the conventional semiclassical approximation or as a diffractive integral [12,28] as implemented in the PSCA. We employ for the latter a combination of the geometric theory of diffraction [35] (GTD) and the uniform theory of diffraction [36,37] (UTD), called GTD-UTD, which has been previously successfully applied for the scattering matrix of the circular billiard [16]. The GTD-UTD takes into account the multiple scattering between the edges of a given lead (for details see Ref. [16]). Second, the quantum propagator is replaced within the PSCA by a semiclassical propagator that contains in addition to classical paths also pseudopaths, i.e., sequences of classical paths joined by diffractive (back) scattering at the lead openings. The reasoning underlying this augmented path manifold is that near the sharp edges of the leads or, more generally, at the interface between the quantum point contacts and the cavity (Fig. 1), the semiclassical regime of sufficiently small λ_{dB} cannot be reached and, therefore, nonclassical path contributions, determined to leading order in $\hbar$ by diffractive integrals, must be included from the outset. These pseudopaths are contributions to the Feynman path integral that are nonclassical in origin, yet can be systematically included in the approximation. Accordingly, each pseudopath p of order $\eta(p)$ consists of a sequence of $\eta+1$ classical path segments p_i joined by η diffractive scatterings at one of the lead openings (or point contacts) with diffractive amplitude $v(\theta^{p_i},\theta^{p_i-1},k)$, where θ^{p_i-1} (θ^{p_i}) are the incoming (outgoing) scattering angle with which the trajectory p_{i-1} (p_i) approaches (leaves) the point contact. Explicit analytic expressions of the coupling coefficient $v(\theta^{p_i},\theta^{p_i-1},k)$ are given in Appendix. The PSCA to the propagation along the pseudopath p between the starting point $\mathbf{r}$ and the end point $\mathbf{r}'$ reads

$$G_p^{\mathrm{PSCA}}(\mathbf{r}',\mathbf{r},k) = \left[\prod_{i=1}^{\eta} G_{p_i}^{\mathrm{SCA}}(k)v(\theta^{p_i},\theta^{p_{i-1}},k)\right] G_{p_0}^{\mathrm{SCA}}(k), \tag{7}$$

where the amplitude for each classical path segment p_i connecting two quantum point contacts is given by the standard SCA expression for the rectangular billiard

$$G_p^{\mathrm{SCA}}(k) = \frac{2\pi}{(2\pi i)^{3/2}}\sqrt{|D_p(k)|} \times \exp\left[iS_p(k) - i\frac{\pi}{2}\mu_p\right] = \frac{2\pi}{(2\pi i)^{3/2}}\frac{1}{\sqrt{kL_p}}\exp[ikL_p - iN_p\pi]. \tag{8}$$

The complete propagator $G_\Lambda^{\mathrm{PSCA}}(\mathbf{r}',\mathbf{r},k)$ to order Λ is the sum over all contributions from pseudopaths connecting $\mathbf{r}'$ and $\mathbf{r}$ with $\eta(p) \leqslant \Lambda$

$$G_\Lambda^{\mathrm{PSCA}}(\mathbf{r}',\mathbf{r},k) = \sum_{p:\eta(p)\leqslant\Lambda} G_p^{\mathrm{PSCA}}(\mathbf{r}',\mathbf{r},k). \tag{9}$$

Note that in Eq. (9) $\mathbf{r}'$ and $\mathbf{r}$ can be arbitrary points inside the billiard. In the application to the wave function [Eq. (4)] we will set $\mathbf{r}$ to be the entrance point contact $\mathbf{r}_1$ and $\mathbf{r}'$ to be an arbitrary internal point inside the billiard while in Eq. (5) $\mathbf{r}'$ is one of the lead-billiard junctions when transmission or reflection is determined. The order Λ controls the degree to which diffractive contributions are included. Since the sum in Eq. (9) extends over infinitely many contributions its numerical evaluation requires in practice the limitation of path lengths by a cutoff length $L_{\max}$. For integrable billiards such as the rectangular billiard the number of trajectories below a maximum length $M^{\mathrm{SCA}}(L_{\max})$ increases quadratically, $M^{\mathrm{SCA}}(L_{\max}) \propto L_{\max}^2$. However, the number of pseudopaths resulting from joining classical paths by a sequence of diffractive couplings eventually proliferates exponentially, $M^{\mathrm{PSCA}}(L_{\max}) \propto \exp(L_{\max}/L_0)$. Therefore, sums over pseudopaths in numerical implementations can only by executed up to modest length $L_{\max}$. The convergence depends on the parameter pair $(\Lambda, L_{\max})$. Note that $G^{\mathrm{PSCA}}_{\Lambda=0}$ [Eq. (9)] is not equivalent to G^{SCA} [Eq. (8)]. In the SCA a path that hits the exit leaves the cavity. Within the PSCA the diffractive scattering at the exit gives rise to a plane wave and, to first order, a circular diffractive wave. In zeroth order the circular wave vanishes but the plane wave leads to geometrically reflected paths, which are not included in the SCA.

The propagator within the PSCA, G^{PSCA}, can be used to construct the semiclassical wave function via Eq. (4). However, the integral over the entrance lead-billiard junction weighted with the transverse mode wave function χ_n would require the calculation of $G^{\mathrm{PSCA}}(\mathbf{r}',x=0,y)$ for all points $-d/2 < y < d/2$. For low mode numbers n we can approximate the integral by a diffraction approximation that replaces the lead junction by a quantum point contact, which acts as a point scatterer located at $\mathbf{r}_1$.

We note that this description is appropriate for low-energy scattering with $\lambda_{\mathrm{dB}} \approx d$ while in the high-energy limit $\lambda_{\mathrm{dB}} \ll d$ entire path bundles emanating from the finite-size lead opening rather than resolved paths connecting the point contacts should be included in the semiclassical approximation [31]. In the following we will focus on paths emitted from such a point contact. The amplitude for a incoming particle in mode n to leave the point contact at the entrance lead with launching angle θ relative to the lead axis (see Fig. 1) and wave number k is denoted by $c_n(\theta,k)$ (see Appendix for its analytic form).

Analogously $c_m^*(\theta,k)$ represents the amplitude for a trajectory incident on the junction under the angle θ to exit in mode m.

Inserting Eq. (9) and $c_n(\theta,k)$ into Eq. (4) yields the PSCA for the scattering wave function inside the billiard subject to the boundary condition [Eq. (1)] of incident current in mode n

$$\Psi_{n,\Lambda}^{\mathrm{PSCA}}(\mathbf{r}',k) = -i\sqrt{k_n} \sum_{p:\eta(p)\leqslant\Lambda} G_p^{\mathrm{PSCA}}(\mathbf{r}',\mathbf{r}_1,k) c_n\left(\theta_p^e,k\right), \quad (10)$$

where θ_p^e is the entrance angle of the trajectory p. Analogously, the transmission amplitude follows as

$$t_{mn}(k) = -i\sqrt{k_m k_n} \sum_{p:\eta(p)\leqslant\Lambda} c_m\left(\theta_p^f,k\right) G_p^{\mathrm{PSCA}}(\mathbf{r}_2,\mathbf{r}_1,k) c_n\left(\theta_p^e,k\right), \quad (11)$$

where θ_p^f is the exit angle of the trajectory p. We will use in the following Eq. (11) as a test for the accuracy of the PSCA complementary to that for the wave function in Eq. (10).

III. QUANTUM CALCULATIONS

Before presenting results of the PSCA, we briefly review the method employed for solving the underlying quantum problem. Our quantum calculations are based on the modular recursive Green's function method (MRGM) [38–40]. In the MRGM the two-dimensional (2D) Schrödinger equation is solved numerically on a tight-binding grid, which leads to a nonquadratic (cosine) dispersion relation. While in the PSCA the dispersion relation has the correct form of $E = k^2/2$, the discretization within the MRGM leads to a nonquadratic (cosine) dispersion relation, the main source for deviations from the exact 2D Schrödinger equation. Thus, the comparison between the PSCA and QM requires small grid spacings within the MRGM. We have used 30 grid points per half-wave length. A coarser discretization below this value leads to a visible shift in k of the QM transport results with respect to the PSCA due to the nonquadratic dispersion relation.

Even though the concept of paths and path lengths does not explicitly enter the quantum description, the scattering wave function $\Psi(\mathbf{r},k)$ can be Fourier analyzed in terms of its length component L,

$$\tilde{\Psi}(\mathbf{r},L) = \int dk \Psi(\mathbf{r},k) e^{-ikL}. \quad (12)$$

As we will show the Fourier conjugate variable to k is closely related to the physical variable length of the (semi)classical dynamics. For the numerical evaluation of Eq. (12), we perform a windowed Fourier transform in interval $[k_{\min},k_{\max}]$.

Equation (12) is the generalization of the path length spectroscopy [6,12,15,41] of S-matrix elements

$$\tilde{S}_{mn}(L) = \int_{k_{\min}}^{k_{\max}} dk\ S_{mn}(k) e^{-ikL}. \quad (13)$$

$\tilde{S}_{mn}(L)$ is the probability amplitude for a quantum path of length L to scatter from mode n to m. The path-length spectrum of open quantum systems decays for increasing length L. However, contributions from very long paths may become important near resonances of long-lived quasibound states. We will present examples of path length distributions entering Ψ below.

Assuming for the moment that the Fourier component $\tilde{\Psi}(\mathbf{r},L)$ can be, indeed, identified with the semiclassical path length, it is now instructive to construct truncated quantum wave functions that retain only Fourier components with L less than the maximum path length $L_{\max}$ included in the PSCA. To this end, we truncated the inverse Fourier transform at $L = L_{\max}$

$$\Psi^{\mathrm{T}}(\mathbf{r},k) = \int_0^{L_{\max}} dL\ \tilde{\Psi}(\mathbf{r},L) e^{ikL}. \quad (14)$$

Analogous truncation of Fourier spectra are performed for S matrix elements

$$S_{mn}^{\mathrm{T}}(k) = \int_0^{L_{\max}} dL\ \tilde{S}_{mn}(L) e^{ikL}. \quad (15)$$

Normalizations have been omitted for simplicity. The comparison between Ψ^{T} and Ψ^{PSCA} allows us to directly and quantitatively compare the semiclassical wave function with the quantum wave function that contains all Feynman paths up to the same length $L_{\max}$. Conversely, comparison between Ψ^{T} and the full quantum wave function Ψ allows us to assess the influence of long paths $L > L_{\max}$ and, therefore, the truncation error involved in semiclassical path sums (see Sec. IV B).

The numerical evaluation of the Fourier transform for finite discretized intervals in k gives rise to a maximal resolvable length $\Delta L = 2\pi/\delta k$ where δk is the grid spacing in the k domain. In order for contributions with $L > L_{\max}$ not to enter Ψ^{T}, the amplitude at the maximum resolvable length ΔL, $\tilde{\Psi}(\mathbf{r},\Delta L)$, must already be strongly suppressed. Otherwise, the Fourier spectrum is back folded such that contributions with $L \gtrsim \Delta L \gg L_{\max}$ appear near the origin ($L \approx 0$) and cannot be cleanly cut off by Eq. (14). To avoid such back folding we choose a large ΔL. However, we will see in Sec. IV B that a complete truncation cannot be established in the vicinity of sharp resonances.

The truncation in L corresponds to the application of a sinc filter in signal processing and results in a finite resolution in k or an effective energy average whose full width at half maximum is given by

$$\sigma = \frac{7.582}{L_{\max}}. \quad (16)$$

By applying the truncation, all details on a finer scale than σ are smeared out leading to a smoothing of sharp peaks as a function of k. Consequently, unitarity is violated since high Fourier components corresponding to contributions from long paths are missing. Note, however, that the convolution is performed on the level of the amplitudes whereas, e.g., in the semiclassical description of scars [29], the energy average is applied to the absolute square of the wave function, i.e., the local density of states. In the latter case the associated effective average window differs approximately by a factor of $1/\sqrt{2}$ (see Fig. 8).

The relative importance of a given path length can be quantified by the expectation value of the Eisenbud-Wigner-Smith

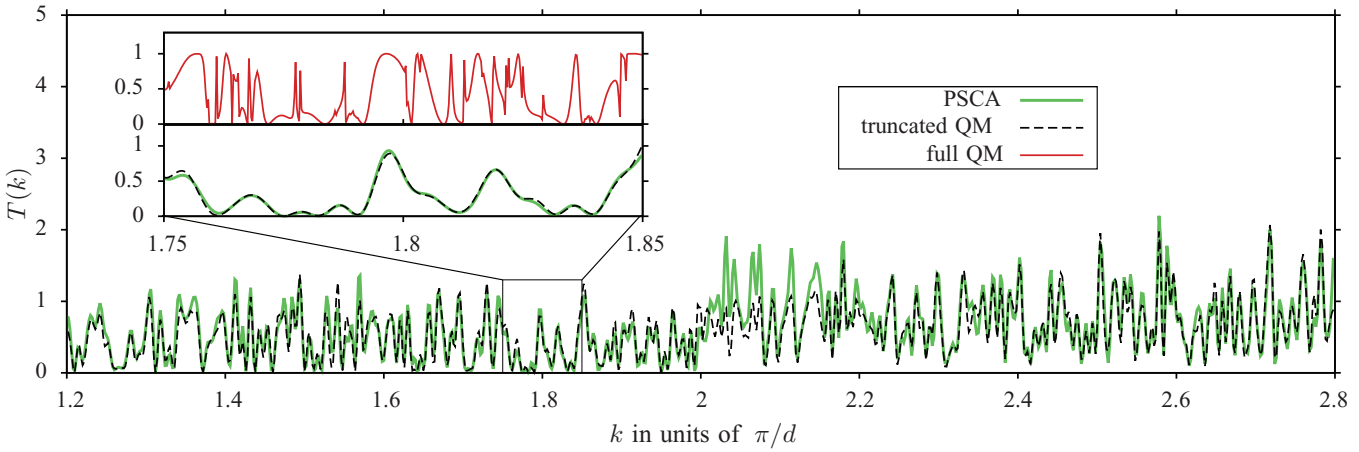

FIG. 2. (Color online) Comparison of the total transmission $T(k)$ as a function of k within the PSCA [green (light gray) line], truncated QM (black dashed line), and full QM [in the inset, upper panel red (dark gray) line]. The PSCA is calculated for a maximum path length of $L_{\max} = 17.5$ and maximum order of diffractive scattering $\Lambda = 6$. The inset shows a magnification of the region $k \in [1.75, 1.85]$.

(EWS) time delay operator for incoming mode n

$$\tau_{\mathrm{EWS}} = \langle Q \rangle = \left\langle -iS^{\dagger}\frac{\partial}{\partial E}S \right\rangle = -i\sum_{m} t^{\dagger}_{nm}\frac{\partial}{\partial E}t_{mn} + r^{\dagger}_{mn}\frac{\partial}{\partial E}r_{mn}. \tag{17}$$

For billiards with zero potential in the interior, the time delay τ_{EWS} can be directly converted into a path length

$$\ell_{\mathrm{EWS}} = k\tau_{\mathrm{EWS}}. \tag{18}$$

By comparing $\ell_{\mathrm{EWS}}(k)$ at a given wave number k with $L_{\max}$ we can provide an independent estimate for the expected proximity of Ψ^{T} to Ψ and, in turn, for the convergence of Ψ^{PSCA} to the full scattering state.

An alternative measure for the time the particle spends inside the cavity is the dwell time

$$\tau_{\mathrm{D}} = \int_{\mathrm{cavity}} |\Psi(\mathbf{r},k)|^2 dx\, dy. \tag{19}$$

The difference between τ_{EWS} and τ_{D} is referred to as the interference delay that the wave packet experiences before entering the cavity due to interference with parts of itself that have already been reflected [42]. This self-interference delay becomes important when the de Broglie wavelength of the particle is comparable to the linear dimension of the billiard. In the semiclassical regime, however, we find $\tau_{\mathrm{D}} = \tau_{\mathrm{EWS}}$ to a very good degree of approximation.

IV. NUMERICAL RESULTS

A. Scattering matrix

To set the stage, we first present typical results for S-matrix elements [Eqs. (5) and (11)]. The total transmission $T(k)$ [Eq. (6)] as a function of the incident energy or, equivalently, k (Fig. 2) displays excellent agreement between the PSCA and the scattering matrix S^{T} truncated at the same path length $L_{\max} = 17.5$ as the PSCA. A few exceptions are worth mentioning. They appear, e.g., in the vicinity of the channel opening $k \gtrsim 2$. Just above the channel opening the emission angle θ is close to $\pi/2$. For grazing incidence the diffraction amplitude $c_n(\theta,k)$ and scattering amplitude $v(\theta',\theta,k)$ in GTD-UTD is less accurate, most likely causing this discrepancy. While, overall, the agreement between the PSCA and the truncated quantum S matrix is remarkable, pronounced differences appear to the full quantum S matrix as highlighted in Fig. 2 for the magnified interval $1.75 \leqslant k \leqslant 1.85$. Pronounced sharp structures are missing in the PSCA indicating that the latter are due to long paths, i.e., represent long-lived resonances. In principle, the PSCA could account for those if $L_{\max}$ could be extended. In practice, however, the exponential proliferation of contributing pseudopaths prevents to perform complete path sums. The comparison suggests that for those k values where sharp resonances appear, the PSCA wave function will be significantly different from the quantum scattering state Ψ while in spectral regions where $T(k)$ is smooth, the PSCA should become accurate.

B. Wave functions

We present in the following three prototypical cases of scattering wave functions: one in the smooth off-resonant part of the spectrum for incoming mode $n = 1$ (Fig. 3), one near a sharp resonance (Fig. 4) and one for incoming mode $n = 2$ (see Fig. 10 below). Obviously, in the nonresonant case we find near perfect agreement between Ψ, Ψ^{T}, and Ψ^{PSCA} while in the resonant case Ψ^{PSCA} strongly differs from Ψ but is in close agreement with Ψ^{T}, as anticipated. In resonant scattering a long-lived quasibound state is excited such that contributions from very long path lengths become essential while off-resonant wave functions typically show signatures associated with the dynamics of short paths.

The computational effort to calculate Ψ^{PSCA} is much larger than for the S-matrix elements since the path sum has to be performed for each grid point of a square lattice with small spacings δx. In order to generate high-resolution images of Ψ^{PSCA} with modest computational effort we employ the following trick: we expand Ψ^{PSCA} in terms of the analytically

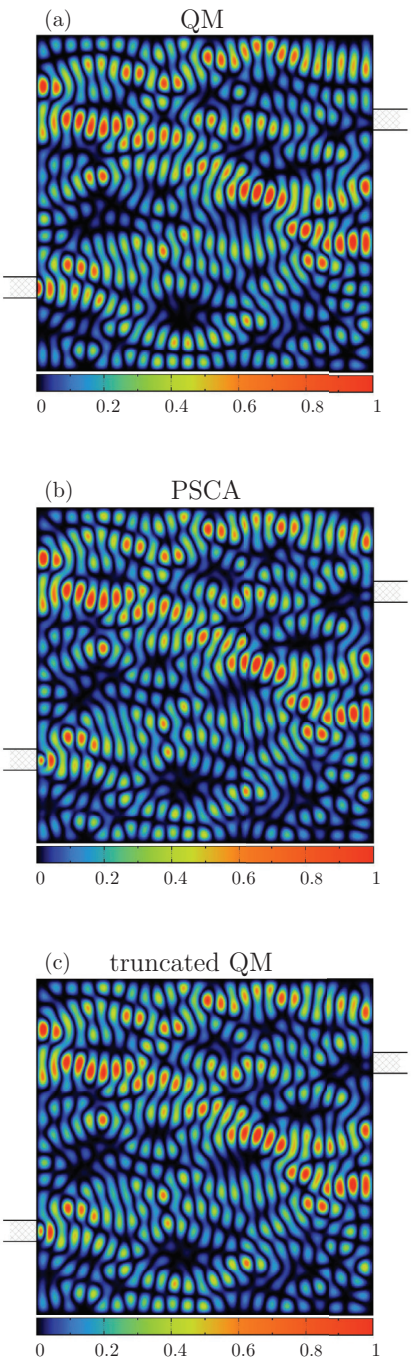

FIG. 3. (Color online) Comparison of the full quantum wave function Ψ, Ψ^{PSCA}, and the truncated wave function Ψ^{T} for a nonresonant scattering state in incident mode $n = 1$ with $k = 1.7835$ and $\ell_{\mathrm{EWS}} = 10.5$. (a) Full quantum wave function Ψ, (b) PSCA with $L_{\max} = 17.5$ and maximum diffractive order $\Lambda = 6$, (c) truncated quantum wave function with Fourier components $L \leqslant L_{\max} = 17.5$.

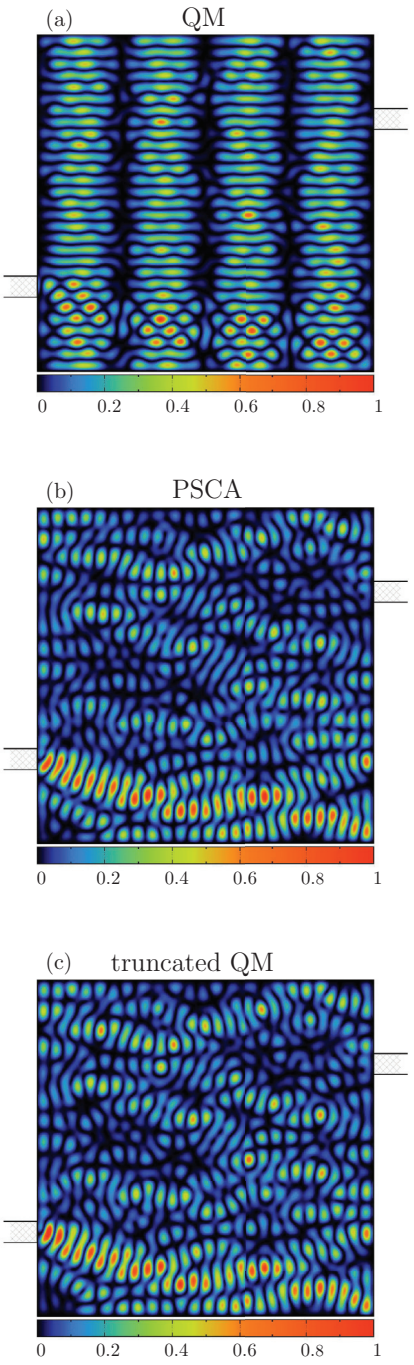

FIG. 4. (Color online) As Fig. 3 but for a resonant scattering state in incident mode $n = 1$ with $k = 1.8295$ and $\ell_{\mathrm{EWS}} = 47$.

known eigenstates of the closed billiard

$$\langle \mathbf{r}|mn\rangle = \frac{2}{D}\sin(K_m x)\sin(K_n y), \tag{20}$$

where $K_n = \frac{\pi}{D}n$. With the help of the projection amplitude

$$a_{mn}^{\mathrm{PSCA}} = \langle mn|\Psi^{\mathrm{PSCA}}\rangle \tag{21}$$

evaluated on the grid, we can evaluate Ψ^{PSCA} in the interior as

$$\Psi^{\mathrm{PSCA}}(\mathbf{r},k) = \frac{2}{D}\sum_{mn} a_{mn}^{\mathrm{PSCA}}(k)\sin(K_m x)\sin(K_n y). \tag{22}$$

Due to energy conservation the expansion coefficients $a_{mn}^{\mathrm{PSCA}}(k)$ are nonzero only near the circle $K_m^2 + K_n^2 = k^2$ (see, e.g., the inset of Fig. 5). In the limit of a bound state of the closed billiard the amplitudes take the form of a delta function $a_{mn}(k) = \delta(k - \sqrt{K_n^2 + K_m^2})$. We can thus use a coarse grid $\delta x \lesssim \pi/k$ such that the maximal resolved wave number $\Delta K =$

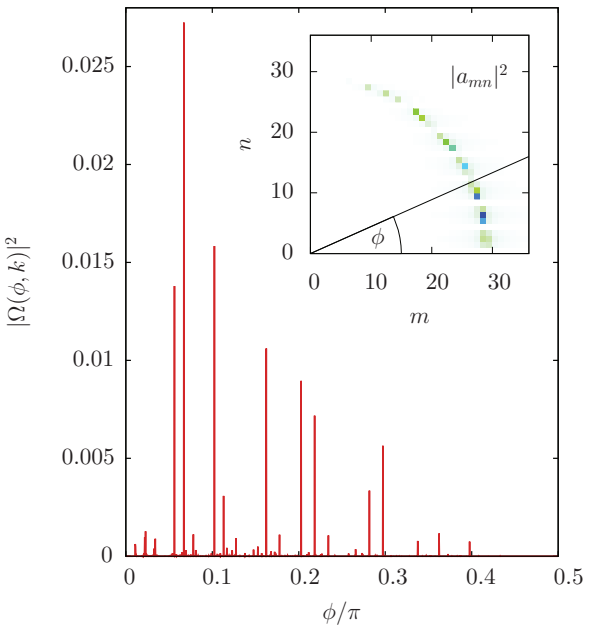

FIG. 5. (Color online) The absolute square of the spectral angular amplitude $\Omega(\phi,k)$ [Eq. (23)] at fixed wave number $k = 1.7835$ for Ψ within full quantum mechanics [Fig. 3(a)]. The inset shows the expansion coefficients $a_{nm}(k)$ and the definition of the angle ϕ. The color code goes from white for vanishing amplitude over green (light gray) to dark blue (dark gray) for maximum amplitude.

$\pi/\delta x$ is slightly larger then the wave number k of the scattering state. $a_{mn}(k)$ calculated from this coarse grid contains the complete information on the wave function inside the cavity. We note that the eigenfunctions of the closed billiard do not form a complete basis for the open billiard because the lead openings are replaced by hard walls. Therefore, the Fourier expansion [Eq. (21)] and its inverse are not strictly unitary.

Since the expansion coefficients a_{mn} are nonzero only near the circle $k^2 = K_m^2 + K_n^2$, we can construct a spectral angular amplitude of the scattering state with wave number k as

$$\Omega(\phi,k) = \sum_{n,m} \delta(n, \tan(\phi)m) a_{mn}(k). \tag{23}$$

The expression $\delta(n, \tan(\phi)m)$ is unity for $\tan(\phi) = n/m$ and zero elsewhere. Equation (23) can be applied to both the exact quantum state and to its semiclassical approximation. Figure 5 shows the angular spectra of the nonresonant scattering state [Fig. 3(a)] within full quantum mechanics. As expected from the visual inspection of the wave function, the angular distribution shows many peaks corresponding to a large number of excited modes. Nevertheless $\Omega(\phi,k)$ is not uniformly distributed in angle ϕ because excitation of modes with large ϕ would lead, in general, to long lifetimes caused by their weak cavity-lead coupling [see Fig. 9(a)]. For states with short dwell times such as in Fig. 3 large ϕ contributions are suppressed.

To quantify the agreement between the quantum and semiclassical wave functions we use the distance metric in Hilbert space

$$d^2(\Psi_1,\Psi_2) = \frac{1}{D^2} \iint_{\text{cavity}} dx\, dy\, |\Psi_2(\mathbf{r},k) - \Psi_1(\mathbf{r},k)|^2. \tag{24}$$

The convergence of the semiclassical wave function Ψ^{PSCA} as a function of Λ and $L_{\max}$ can be conveniently studied by employing $d^2(\Psi^{\text{T}},\Psi^{\text{PSCA}})$. We observe that at fixed $L_{\max}$ and increasing Λ, Ψ^{PSCA} converges monotonically to Ψ^{T} shown in Fig. 6(a) for the scattering state at $k = 1.7835$.

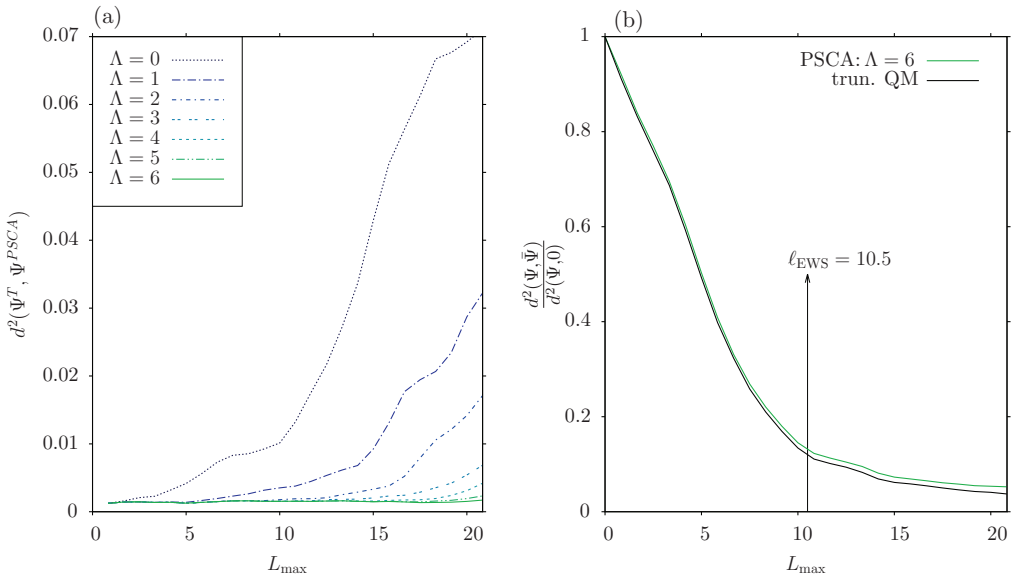

FIG. 6. (Color online) (a) The distance $d^2(\Psi^{\text{PSCA}},\Psi^{\text{T}})$ as a function of $L_{\max}$ depicted for varying orders $\Lambda = 1$ to $\Lambda = 6$ and wave number $k = 1.7835$ (same as in Fig. 3). (b) The normalized distance, $\frac{d^2(\Psi,\bar{\Psi})}{d^2(\Psi,0)}$, of $\bar{\Psi}$ to the exact quantum wave function Ψ, with $\bar{\Psi}$ being either Ψ^{PSCA} [green (light gray) line] or Ψ^{T} (black line) as a function of $L_{\max}$ for the same wave number as in (a). The mean path length within the full QM [Eq. (18)] is $\ell_{\text{EWS}} = 10.5$ and is marked by a vertical line. The PSCA is depicted for order $\Lambda = 6$. Ψ^{T} (black line) is obtained via a discrete Fourier transform of Eq. (14) in the interval $k \in [1.725, 1.875]$ with $\delta k = 0.00025$.

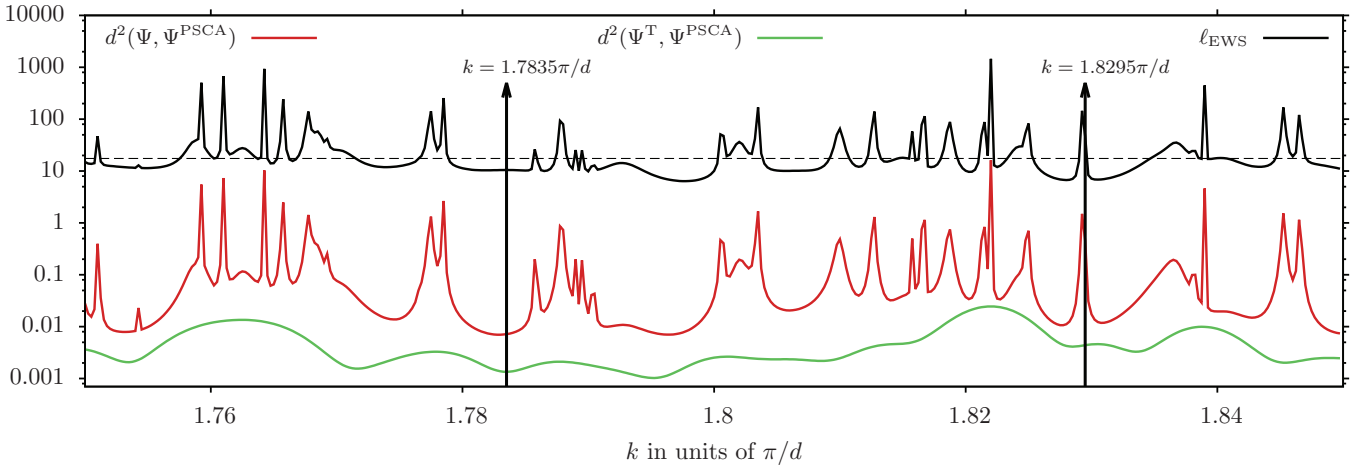

FIG. 7. (Color online) Distance $d^2(\Psi,\Psi^{\rm PSCA})$ between the quantum wave functions Ψ and the PSCA $\Psi^{\rm PSCA}$ [red (dark gray) line], as well as the distance $d^2(\Psi^{\rm T},\Psi^{\rm PSCA})$ between the truncated QM and the PSCA [green (light gray) line]. The PSCA is calculated to order $\Lambda=6$ with $L_{\rm max}=17.5$. The black solid line is the mean path length $\ell_{\rm EWS}$ [see Eq. (18)] and the horizontal dashed line marks a mean path length of $\ell=L_{\rm max}=17.5$. Note the logarithmic scale of the figure. The two vertical arrows mark the wave number of a nonresonant scattering state ($k=1.7835$, as in Fig. 3) and the wave number of a resonant scattering state ($k=1.8295$, Fig. 4), respectively. The sharp peak at $k=1.82925$ corresponds to the resonance $m=29,n=4$ and has a mean path length of $\ell_{\rm EWS}=145$ almost degenerate to the resonance state $m=4,n=29$ at $k=1.8295$.

The semiclassical wave function $\Psi^{\rm PSCA}$ has converged to Ψ^T within $d^2(\Psi^{\rm T},\Psi^{\rm PSCA})=0.0015$ for $\Lambda=6$ at $L_{\rm max}=20$.

At fixed Λ and increasing $L_{\rm max}$ the semiclassical wave function $\Psi^{\rm PSCA}$ starts to diverge from $\Psi^{\rm T}$ with the onset of divergence shifted to larger $L_{\rm max}$ as Λ increases [Fig. 6(a)]. This is a consequence of the increasing lack of pseudopaths required for the complete path sum at length $L_{\rm max}$. For large $L_{\rm max}$ an exponentially increasing number of pseudopaths of the same length become accessible that consist of segments of shorter classical paths joined by an increasing number of diffractive scatterings [see Eq. (7)]. Some of these high-order pseudopaths are missing for the proper interference with the paths already included in the PSCA of low order Λ. Therefore, convergence to the quantum wave function, if existent, requires a correlated limit of both large $L_{\rm max}$ and Λ. It should be noted that with increasing order Λ, the PSCA becomes more and more sensitive to the accuracy of $v(\theta',\theta,k)$ (the diffractive amplitude for the internal scattering at the cavity-lead junction) since any error in $v(\theta',\theta,k)$ is exponentiated to the power Λ. We note parenthetically, that the global convergence of the (pseudo)path sum, in particular near sharp resonances and for weakly open structures, remains an open question.

While the dependence of $d^2(\Psi^{\rm T},\Psi^{\rm PSCA})$ on the order Λ of the PSCA allows to estimate the significance of diffractive contributions to the path sum up to a given length $L_{\rm max}$, the distance $d^2(\Psi,\Psi^{\rm T})$ measures the total contribution of paths with length beyond $L_{\rm max}$ [Fig. 6(b)]. The convergence of $\Psi^{\rm T}$ to the exact scattering state as a function of $L_{\rm max}$ is controlled by the mean path length $\ell_{\rm EWS}$ of the exact scattering state. In general, for $L_{\rm max}\gtrsim\ell_{\rm EWS}$ the truncated wave function $\Psi^{\rm T}$, and thereby $\Psi^{\rm PSCA}$ for sufficiently high Λ converge to the full scattering state.

The PSCA fails to reproduce the quantum scattering state near a sharp resonance (Fig. 4) because long paths well beyond $L_{\rm max}$ contribute to the long-lived quasibound state. It is therefore instructive to directly compare the distance functions $d^2(\Psi,\Psi^{\rm PSCA})$ with the EWS length $\ell_{\rm EWS}$ as a function of k (Fig. 7). Indeed, the distance of the wave function in Hilbert space strongly correlates with the mean path length $\ell_{\rm EWS}$ and allows to predict the accuracy of $\Psi^{\rm PSCA}$ for a given $L_{\rm max}$ when $\ell_{\rm EWS}$ is known. The two prototypical cases shown above are marked in Fig. 7. It is also instructive to measure the distance between $\Psi^{\rm PSCA}$ and $\Psi^{\rm T}$ (Fig. 7). It is uniformly small (<0.05) over the entire k interval and slowly varying. It is worth noting that the residual fluctuations in $d^2(\Psi^{\rm T},\Psi^{\rm PSCA})$ are not due to shortcomings of the PSCA but rather due to the truncation process in $\Psi^{\rm T}$ [see Eq. (14)]. Near resonances $\tilde{\Psi}(\mathbf{r},L)$ contains non-negligible contributions up to very long paths. Consequently, when $\tilde{\Psi}(\mathbf{r},L)$ is still non-negligible for L beyond the Fourier resolution limit $L>\Delta L=2\pi/\delta k$, back folding causes truncation errors. The latter are responsible for the increase of $d^2(\Psi^{\rm T},\Psi^{\rm PSCA})$ in the region of high density of sharp resonances (e.g., near $k=1.765$ and $k=1.822$).

The contribution from long paths and the possible contamination by back folding can be conveniently monitored by the projection amplitudes $a_{mn}(k)$ onto bound states of the closed billiard [Eq. (21)] or onto quasibound states of the open billiard. We present $|a_{mn}(k)|^2$ and its path length spectrum $|\tilde{a}_{mn}(L)|^2$, where

$$\tilde{a}_{mn}(L)=\int dk\; a_{mn}(k)e^{-ikL} \tag{25}$$

for two extreme cases in Fig. 8, the broad resonance ($m=29$, $n=1$) and the sharp resonance ($m=15$, $n=25$). For the broad resonance, the PSCA and the truncated quantum state agree perfectly since the path length spectrum of the amplitude has already decayed by over four orders of magnitude near $L=\Delta L=500$. For the sharp resonance with $\ell_{\rm EWS}=1460$, the path length spectral intensity at $L\approx500$ is still $\approx10^{-1}$ of its value for small L and, consequently, truncation leads to large discrepancies between $\Psi^{\rm PSCA}$ and $\Psi^{\rm T}$. Naturally both the PSCA and the quantum state truncated at $L_{\rm max}=17.50$

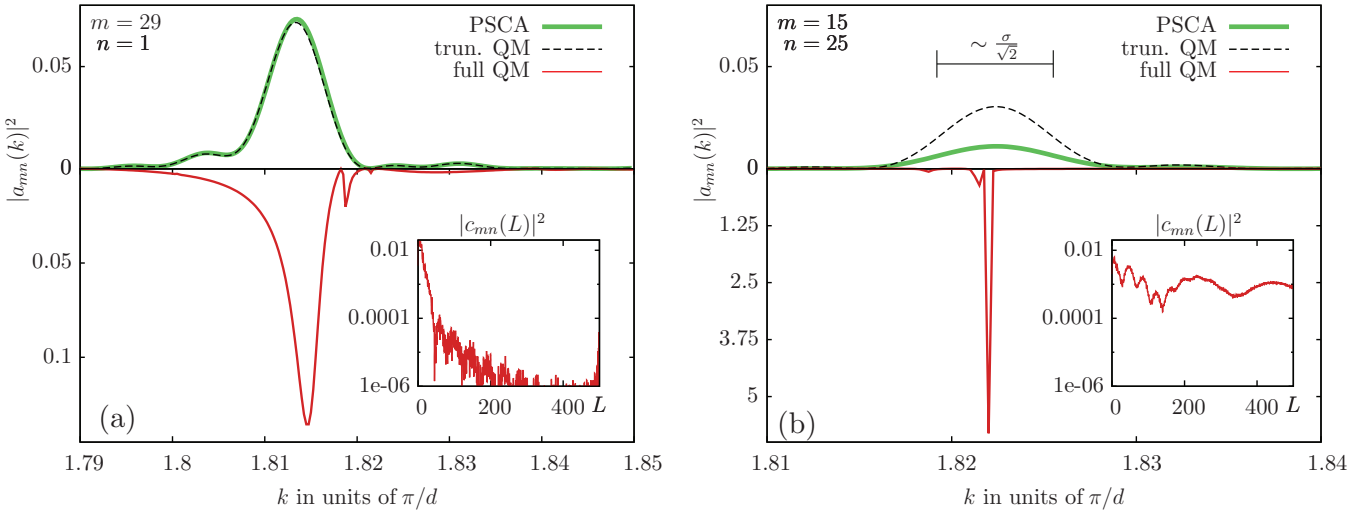

FIG. 8. (Color online) The absolute magnitude square of the amplitudes $|a_{mn}(k)|^2$ for the two extreme cases of (a) a broad resonance ($m = 1,n = 29$) and (b) a sharp resonance ($m = 25,n = 15$). Note the different ranges of the ordinate in (a) and (b) for the quantum result. The inset shows the length spectrum $|a_{mn}(L)|^2$ of the amplitude of Ψ on a logarithmic scale. The length spectrum of the sharp resonance [inset of (b)] is not sufficiently decreased at the boundary of numerical resolution $\Delta L = 500$ such that some paths with $L > L_{\max}$ are not filtered out of Ψ^{T}. This causes the difference between Ψ^{T} (black dashed line) and Ψ^{PSCA} [green (light gray) line] in (b). The scattering state which excites the sharp resonance corresponds to the mean path length of $\ell = 1460$ at $k = 1.822$ (see Fig. 7). The scale bar gives the width $\sigma/\sqrt{2} = 0.0061\pi/d$ of the effective energy average associated with the truncation on the level of the square absolute amplitudes [for σ see Eq. (16)]. The PSCA is calculated with $L_{\max} = 17.5$ and order $\Lambda = 6$.

fail to describe the exact quantum scattering state for the sharp resonance.

The visual proximity of quantum scattering states near long-lived resonances to bound states of the closed system [Fig. 4(a)] might suggest that they can be approximated by semiclassical wave functions of the closed system. However, the amplitude with which such a scattering resonance is excited by the incoming scattering state is essentially controlled by the diffractive coupling to the asymptotic incoming and outgoing scattering states at the lead entrance and exit. Moreover, while the position k_R of the resonance can be estimated from the quantized closed system [43–45], its width Γ and its Fano asymmetry parameter [46] can only be determined within a semiclassical description of the open billiard. Inclusion of very long paths into the latter remains a challenge. Only in exceptional cases such as the hyperbolic three-disk problem with only isolated unstable periodic orbits the line width of scattering resonances could be determined by a rapidly convergent cycle expansion of the spectral determinant [47–49]. Such an approach is not directly applicable to the integrable billiard with a continuous manifold of (stable) periodic orbits. We emphasize that the case of narrow resonances where the numerical evaluation of the PSCA fails is the exception rather than the rule. For example, 92% of the scattering states in Fig. 7 have a mean path length ℓ_{EWS} of less than 50. Only 8% are associated with long-lived resonances. Moreover, as discussed below, in experimental realizations with decoherence present, the contribution of long paths is suppressed.

While the previous numerical examples feature low wave numbers $k < 2$ with only one open channel we have checked on the convergence of Ψ^{PSCA} for higher wave numbers up to $k = 5$ as well. We find, in general, the same very good agreement between the PSCA and the full quantum mechanics in the regime $L_{\max} > \ell_{\mathrm{EWS}}$ and between the PSCA and the truncated quantum mechanics in the regime $L_{\max} < \ell_{\mathrm{EWS}}$.

An example for the wave function convergence for the second mode with $k = 2.25375$ and $\ell_{\mathrm{EWS}} = 9.5$ is shown in Fig. 10. One remarkable feature of this wave function different from the previous cases is the intensity enhancement along a classical periodic orbit. Both Ψ^{PSCA} and Ψ^{T} show clear traces of this orbit. For the full quantum state Ψ the occurrence of this structure is caused by the excitation with nearly equal amplitude of two almost degenerate eigenstates of the closed system $|m_i,n_i\rangle$ with $m_1 = 26,n_1 = 25$ and $m_2 = 30,n_2 = 20$. Superposition of these two eigenstates lead to an envelope that follows the track of the periodic orbit similar to the formation of a beat in acoustics [50]. It is now instructive to analyze their appearance within the PSCA. We first note that the angular spectrum of Ψ (analogous to Fig. 9) features two dominant peaks with equal height near the angles $\phi_i = \tan^{-1}(n_i/m_i)$ $(i = 1,2)$ determined by the quantum numbers of the two resonant states. Moreover the angular distribution for diffractive coupling from the point contact into the billiard in second mode $c_2(\theta,k)$ [Eq. (10)] features a high amplitude near these angles, $\theta^e = \phi_i$. This differs from the coupling in first mode for which large angles would be suppressed. The buildup of the beat pattern results now from the constructive interference between the rays emitted from the contact into the billiard with entrance angle close to ϕ_i and its replica propagating into the same direction after four consecutive reflections at the billiard wall. The path length difference between two such trajectories inside the billiard is given by

$$\Delta L = 2D\frac{1+\tan\phi_i}{\sqrt{1+\tan^2\phi_i}} = 2D\frac{m_i+n_i}{\sqrt{m_i^2+n_i^2}}. \qquad (26)$$

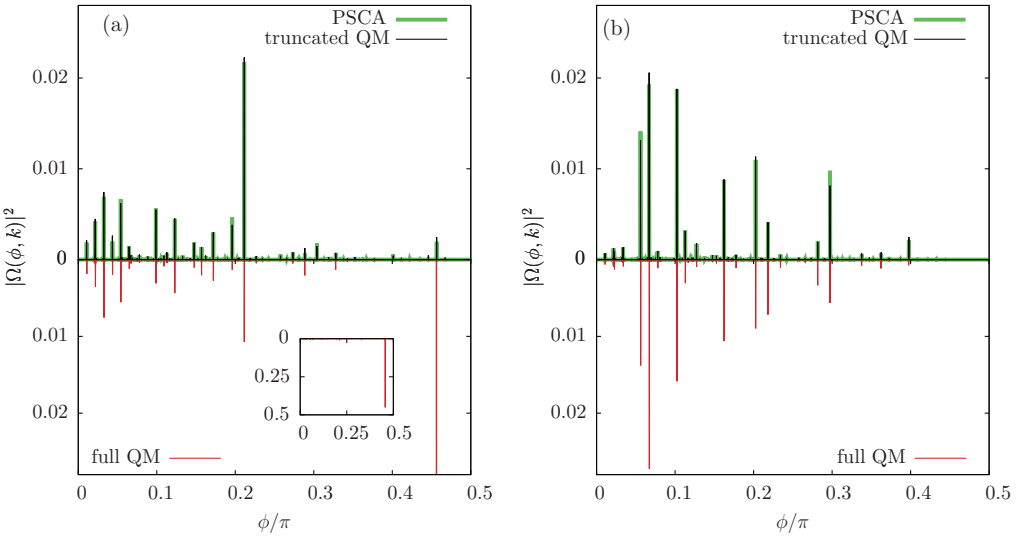

FIG. 9. (Color online) Comparison of $\Omega(\phi,k)$ within PSCA, truncated QM and full QM for (a) a resonant ($k = 1.8295$, Fig. 4) and (b) a nonresonant ($k = 1.7835$, Fig. 3) scattering state. The wave numbers correspond to those labeled in Fig. 7. $L_{\max} = 17.5$, $\Lambda = 6$.

The necessary condition for constructive interference

$$\Delta S = k\Delta L = 2\pi j \ (j \in \mathbb{N}) \tag{27}$$

is now approximately satisfied for both ϕ_1 ($k\Delta L = 100.01\pi$) and ϕ_2 ($k\Delta L = 101.97\pi$) at $k = 2.25375$. In addition, the condition for constructive interference between the rays with entrance angle $\theta^e = \phi_i$ and $\theta^e = -\phi_i$ leads to $\sin(hk_y) = 0$, which gives a simple estimate for the strength of the coupling between eigenstate and incoming second mode (for definition of h see Fig. 1). Both requirements are approximately met for $(m_i,n_i)_{i=1,2}$ resulting in the simultaneous excitation of the corresponding eigenstates and, in turn, in the beat pattern and in the density enhancement near the periodic orbit. The strong coupling between the incident mode $n = 2$ and the two eigenstates is facilitated by the spatial proximity, to within a de Broglie wavelength, of one reflection point of the periodic orbit and the location of the entrance lead.

The excitation amplitude of the eigenstate also depends on the position of the exit lead. Taking into account higher-order diffractive corrections incorporates the coupling to the exit lead into the semiclassical description. Note that the present mechanism for the formation of this periodic orbit is different from the appearance of scars in wave functions of open chaotic billiards for low k [51], which is based on constructive interference for consecutive retracing of a single isolated periodic orbit. It is also different from the appearance of path bundles for large k where bundles of short classical scattering trajectories emanating from the entrance opening whose width is determined by the lead width appear in scattering states [31,52].

The comparison between the truncated and the full QM wave function (Fig. 10) shows that there are nonvanishing contributions from paths with length $L > L_{\max}$ indicating the presence of resonances in the immediate vicinity. Investigation of $d^2(\Psi,\Psi^{\mathrm{T}})$ as function of the truncation length $L_{\max}$ shows rapid decay for small $L_{\max}$ and a slow, plateaulike, decay for $L_{\max} > 11$ due to the residual influence of nearby resonances, which causes a small ℓ_{EWS} but still nonvanishing distance $d^2(\Psi,\Psi^{\mathrm{T}})$ at $L_{\max} = 17.5 > \ell_{\mathrm{EWS}}$.

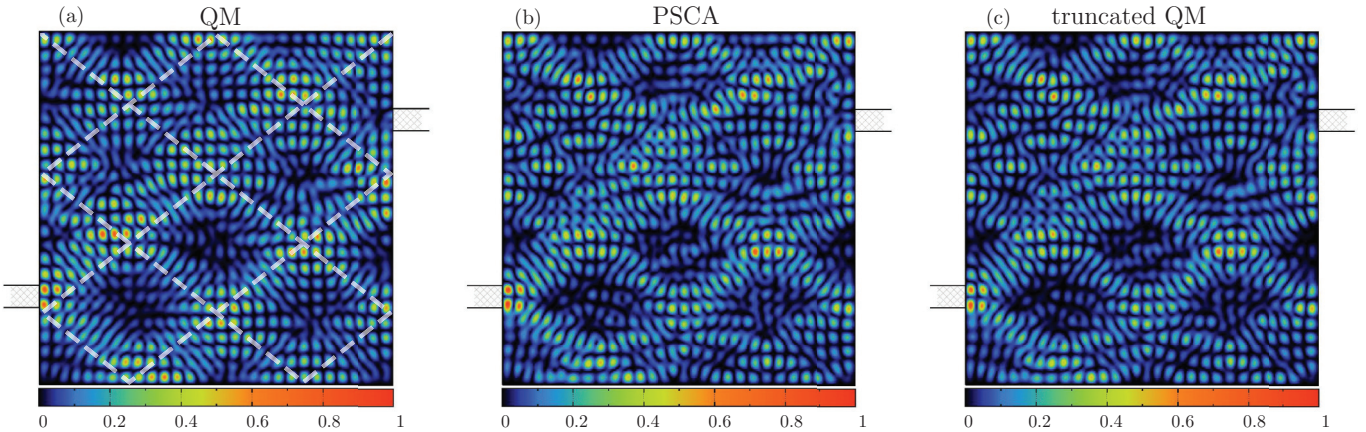

FIG. 10. (Color online) As Fig. 3 but for an off-resonant scattering state in incident mode $n = 2$ with $k = 2.25375$ and $\ell_{\mathrm{EWS}} = 9.5$. Comparison of Ψ, Ψ^{PSCA}, and the truncated wave function Ψ^{T}. The white dashed line in (a) shows the density enhancement along the classical periodic orbit.

V. SUMMARY AND OUTLOOK

We have presented the construction of the semiclassical constant energy propagator and of scattering states employing the pseudopath semiclassical approximation (PSCA). The convergence of the PSCA to the quantum limit is controlled by the maximum path length $L_{\max}$ and the maximum order Λ of nonclassical diffractive scatterings included. For the open rectangular billiard we find unprecedented quantitative agreement between Ψ^{PSCA} and the full quantum scattering state Ψ when the mean path length $\ell_{\mathrm{EWS}} = k\tau_{\mathrm{EWS}}$ determined by the Eisenbud-Wigner-Smith (EWS) time delay τ_{EWS} is covered by the PSCA, $\ell_{\mathrm{EWS}} \lesssim L_{\max}$. Thus, the pseudopaths resulting from sequences of classical paths joined by nonclassical diffractive scatterings at the lead openings provide the necessary complements to the classical paths for completion of the Feynman path sum for quantum propagation. We have presented a protocol for constructing semiclassical scattering wave functions whose convergence to its quantum counterpart can be quantitatively controlled. Even when the mean path length of the exact scattering state ℓ_{EWS} exceeds the maximum path length included in the numerical implementation of the PSCA as it happens for energies (or wave numbers k) near long-lived resonances, we find near-perfect agreement between Ψ^{PSCA} and the corresponding quantum wave function Ψ^{T} with the path length spectrum truncated at the same $L_{\max}$ as the PSCA.

Extension of the present PSCA to the description of scattering states in open chaotic billiards is of considerable interest. However, performing a complete path sum up to a given length poses a challenge as in this case already the set of classical paths [i.e., the zeroth-order ($\Lambda = 0$) diffraction contributions] exponentially proliferates. Combining these classical paths with the exponentially increasing number of pseudopaths when higher-order diffraction corrections are included results in a path set, which will be difficult to enumerate for all but the shortest cutoff length $L_{\max}$. One feature that could possibly simplify this task is a faster convergence of the path sum as a function of the diffractive order compared to integrable systems. For the latter, large Λ are required to generate a sufficient number of pseudopaths to shadow long paths by destructive interference [14]. Exponential proliferation of classical paths may alleviate this problem and lead to accelerated convergence already for smaller Λ.

Due to the mathematical equivalence between the Schrödinger and the Helmholtz equations the experimental measurement of wave functions can be conducted in open microwave billiards using movable antennas [53] or in microcavity lasers [50]. The direct measurement of wave functions in quantum dots is still a major challenge but some progress has been made using scanning tunneling microscopy in graphene quantum dots [54]. The truncation of long paths beyond $L_{\max}$, introduced here to control the sum over an exponentially proliferating set of pseudopaths, does have, in fact, experimental analogues and applications: finite energy resolution of the detection and/or excitation processes leading to smearing out of the sharp resonances is equivalent to suppressing long paths in the expectation value $\langle|\Psi(\mathbf{r})|^2\rangle_E$. Moreover, the finite phase coherence length ℓ_ϕ present in decohering systems precludes the appearance of long-lived resonances and causes long paths to contribute only incoherently [7,55,56]. The latter can easily be incorporated within the PSCA by an exponential damping e^{-L/ℓ_ϕ} of long path contributions [6]. Damping of long paths naturally occurs in billiards with leaky boundary conditions where tunneling through the billiard walls is present. In the experiment such systems can be realized as microwave billiards with dielectric boundaries. The PSCA can be used to describe such systems by incorporating an additional reflection amplitude for each bounce off the billiard walls accounting for the tunneling probability. For such billiards, violation of flux conservation (unitarity) as well as a small mean path length, both naturally incorporated within the PSCA, are key features of the scattering system. The appearance of total reflection for small incident angles causes the reflection amplitude to become a pure phase factor, i.e., its modulus is unity. In the ray picture the associated phase shift can be interpreted by a spatial shift known as the Goos-Hänchen shift [57,58]. The inclusion of this effect can lead to a considerable change in the dynamics of billiards with penetrable walls [59–62]. Due to the possibility of controlling individual path contributions, the PSCA has the potential to develop into an accurate method for calculating scattering states in open billiards where both diffraction at lead edges and dielectric boundary conditions are present.

ACKNOWLEDGMENTS

We thank Philipp Ambichl, Stefan Rotter, and Ludger Wirtz for helpful discussions. This work was supported by the FWF doctoral program "CoQuS". Support by SFB 041-Vicom and the project 23359 of the FWF is gratefully acknowledged. Calculations have been performed on the Vienna Scientific Cluster 1.

APPENDIX: DIFFRACTION AMPLITUDES

We reproduce here the diffraction amplitudes $v(\theta',\theta,k)$ and $c_m(\theta,k)$ within the GTD-UTD. The derivation can be found in Ref. [16].

The diffraction amplitude $v^{\mathrm{GTD}}(\theta',\theta,k)$ for backscattering into the cavity within the GTD [35] is given by

$$v^{\mathrm{GTD}}(\theta',\theta,k,d) = \tfrac{1}{2} D_L(\theta',\theta) e^{-ik\frac{d}{2}(\sin\theta'+\sin\theta)} + \tfrac{1}{2} D_R(\theta',\theta) e^{+ik\frac{d}{2}(\sin\theta'+\sin\theta)} \quad \text{(A1)}$$

with the scattering coefficients at the left and right wedge

$$\begin{aligned} D_L(\theta',\theta) &= D(\pi/2-\theta',\pi/2-\theta) \\ D_R(\theta',\theta) &= D(\pi/2+\theta',\pi/2+\theta) \end{aligned} \quad \text{(A2)}$$

and

$$D(\phi',\phi) = -2\frac{\sin\pi/N}{N}\left[\frac{1}{\cos\frac{\pi}{N}-\cos\frac{\phi'-\phi}{N}} - \frac{1}{\cos\frac{\pi}{N}-\cos\frac{\phi'+\phi}{N}}\right] \quad \text{(A3)}$$

with $N = 3/2$ the exterior angle (in units of π) of a perpendicular wedge. The angles θ and θ' are depicted in Fig. 1. We use the diffraction coefficient within the UTD [36] to take into account multiple scatterings between the two wedges of the

cavity-lead junction

$$D^{\mathrm{UTD}}(\phi',\phi,r',r,k) = -\frac{e^{i\frac{\pi}{4}}}{N}\sum_{\sigma,\eta=\pm1}\sigma\cot\left(\frac{\pi+\eta(\phi'-\sigma\phi)}{2N}\right) \times\left(k\frac{rr'}{r+r'}a_\eta(\phi'-\sigma\phi)\right), \tag{A4}$$

where $a_\pm(\beta) = 2\cos^2(\frac{2\pi Nn^\pm-\beta}{2})$ and $n^\pm$ is the integer that most closely satisfies $2\pi Nn^\pm-\beta=\pm\pi$. The function F is defined as a generalized Fresnel integral

$$F(x) = -2i\sqrt{x}e^{-ix}\int_{\sqrt{x}}^{\infty}d\tau e^{i\tau^2}. \tag{A5}$$

With the notation

$$\begin{aligned} U_L(\theta',\theta,r,k) &= D^{\mathrm{UTD}}(\pi/2-\theta',\pi/2-\theta,r'\to\infty,r,k)\\ U_R(\theta',\theta,r,k) &= D^{\mathrm{UTD}}(\pi/2+\theta',\pi/2+\theta,r'\to\infty,r,k) \end{aligned} \tag{A6}$$

we obtain for the diffraction amplitude $v(\theta',\theta,k)$ within the GTD-UTD

$$\begin{aligned} &v(\theta',\theta,k,d)\\ &\quad= v^{\mathrm{GTD}}(\theta',\theta,k,d)\\ &\qquad+\frac{1}{4}\sum_{\text{odd: j=1}}^{j_{\max}}U_L(\theta',-\pi/2,jd,k)g_j(k)e^{i\Phi^{-+}}D_R(+\pi/2,\theta)\\ &\qquad+U_R(\theta',+\pi/2,jd,k)g_j(k)e^{i\Phi^{+-}}D_L(-\pi/2,\theta)\\ &\qquad+\frac{1}{4}\sum_{\text{even: j=1}}^{j_{\max}}U_R(\theta',+\pi/2,jd,k)g_j(k)e^{i\Phi^{++}}D_R(+\pi/2,\theta)\\ &\qquad+U_L(\theta',-\pi/2,jd,k)g_j(k)e^{i\Phi^{--}}D_L(-\pi/2,\theta), \end{aligned} \tag{A7}$$

where

$$g_j(k) = \frac{1}{\sqrt{2\pi kjd}}\frac{1}{2^{j-1}}e^{i(kjd+(j-1)\pi)} \tag{A8}$$

and

$$\Phi^{\pm\pm} = k\frac{d}{2}(\pm\sin\theta'\pm\sin\theta). \tag{A9}$$

The sum goes over multiples of scatterings between the wedges and is cut at $j_{\max}$ where convergence is reached. We use $j_{\max}=5$.

The diffraction amplitude for coupling of the quantum lead to a cavity within the GTD is given by

$$c_m^{\mathrm{GTD}}(\theta,k,d) = \frac{-ie^{\frac{im\pi}{2}}}{\sqrt{2d}k_{x,m}}\left[\frac{1}{2}D_L(\theta,\theta_m)e^{i\frac{m\pi}{2}}e^{-ik\frac{d}{2}\sin\theta} -\frac{1}{2}D_R(\theta,\theta_m)e^{-i\frac{m\pi}{2}}e^{ik\frac{d}{2}\sin\theta}\right]. \tag{A10}$$

As before we use the notation

$$\begin{aligned} D_L(\theta,\theta_m) &= D\left(\frac{\pi}{2}-\theta,\frac{3\pi}{2}-\theta_m\right),\\ D_R(\theta,\theta_m) &= D\left(\frac{\pi}{2}+\theta,\frac{3\pi}{2}-\theta_m\right) \end{aligned} \tag{A11}$$

for the left and right wedge. The angle θ_m is determined by the open lead mode and is given by $\theta_m=\arcsin(m\pi/dk)$. Using the UTD Eq. (A6) for the out-coupling into the cavity we obtain

$$\begin{aligned} &c_m^{\mathrm{GTD-UTD}}(\theta,k,d)\\ &\quad= c_m^{\mathrm{GTD}}(\theta,k,d) - i\frac{e^{\frac{im\pi}{2}}}{\sqrt{2d}k_{x,m}}\\ &\qquad\times\frac{1}{4}\left[\sum_{\text{odd:j=1}}^{j_{\max}}U_R(\theta,+\pi/2,jd,k)g_j(k)e^{i\phi^{++}}D_L(-\pi/2,\theta_m)\right.\\ &\qquad-U_L(\theta,-\pi/2,jd,k)g_j(k)e^{i\Phi^{--}}D_R(+\pi/2,\theta_m)\\ &\qquad+\sum_{\text{even:j=1}}^{j_{\max}}(-1)U_R(\theta,+\pi/2,jd,k)g_j(k)e^{i\Phi^{+-}}D_R(+\pi/2,\theta_m)\\ &\qquad\left.+U_L(\theta,-\pi/2,jd,k)g_j(k)e^{i\Phi^{-+}}D_L(-\pi/2,\theta_m)\right], \end{aligned} \tag{A12}$$

where

$$\Phi^{\pm\pm} = \pm k\frac{d}{2}\sin\theta\pm\frac{m\pi}{2}, \tag{A13}$$

and $g_j(k)$ is given in Eq. (A8).

[1] P. Dirac, Phys. Z. Sowjetunion **3**, 64 (1933).
[2] R. P. Feynman, Rev. Mod. Phys. **20**, 367 (1948).
[3] C. W. J. Beenakker, Rev. Mod. Phys. **69**, 731 (1997).
[4] S. Datta, *Electronic Transport in Mesoscopic Systems* (Cambridge University Press, Cambridge, 1995).
[5] E. Akkermans and G. Montambaux, *Mesoscopic Physics of Electrons and Photons* (Cambridge University Press, Cambridge, 2006).
[6] H. Ishio and J. Burgdörfer, Phys. Rev. B **51**, 2013 (1995).
[7] T. Blomquist and I. V. Zozoulenko, Phys. Rev. B **61**, 1724 (2000).
[8] M. Brack and R. K. Bhaduri, *Semiclassical Physics,* Frontiers in Physics (Westview Press, Boulder, 2003).
[9] R. Blümel and U. Smilansky, Phys. Rev. Lett. **64**, 241 (1990).
[10] H. U. Baranger, R. A. Jalabert, and A. D. Stone, Chaos **3**, 665 (1993).
[11] T. Blomquist and I. V. Zozoulenko, Phys. Rev. B **64**, 195301 (2001).
[12] L. Wirtz, J.-Z. Tang, and J. Burgdörfer, Phys. Rev. B **56**, 7589 (1997).
[13] L. Wirtz, J.-Z. Tang, and J. Burgdörfer, Phys. Rev. B **59**, 2956 (1999).
[14] L. Wirtz, C. Stampfer, S. Rotter, and J. Burgdörfer, Phys. Rev. E **67**, 016206 (2003).
[15] C. Stampfer, S. Rotter, J. Burgdörfer, and L. Wirtz, Phys. Rev. E **72**, 036223 (2005).
[16] I. Březinová, L. Wirtz, S. Rotter, C. Stampfer, and J. Burgdörfer, Phys. Rev. B **81**, 125308 (2010).

[17] I. Březinová, C. Stampfer, L. Wirtz, S. Rotter, and J. Burgdörfer, Phys. Rev. B **77**, 165321 (2008).
[18] S. Rahav and P. W. Brouwer, Phys. Rev. B **73**, 035324 (2006).
[19] S. Rahav and P. W. Brouwer, Phys. Rev. Lett. **95**, 056806 (2005).
[20] P. Jacquod and R. S. Whitney, Phys. Rev. B **73**, 195115 (2006).
[21] K. Richter and M. Sieber, Phys. Rev. Lett. **89**, 206801 (2002).
[22] P. Braun, S. Heusler, S. Müller, and F. Haake, J. Phys. A. **39**, L159 (2006).
[23] S. Heusler, S. Müller, P. Braun, and F. Haake, Phys. Rev. Lett. **96**, 066804 (2006).
[24] P. W. Brouwer and S. Rahav, Phys. Rev. B **74**, 085313 (2006).
[25] P. Pichaureau and R. A. Jalabert, Eur. Phys. J. B **9**, 299 (1999).
[26] E. Bogomolny, Nonlinearity **13**, 947 (2000).
[27] H. J. Stöckmann, *Quantum Chaos: An Introduction* (Cambridge University Press, Cambridge, 2006).
[28] C. D. Schwieters, J. A. Alford, and J. B. Delos, Phys. Rev. B **54**, 10652 (1996).
[29] E. Bogomolny, Physica D: Nonlinear Phenomena **31**, 169 (1988).
[30] R. Höhmann, U. Kuhl, H.-J. Stöckmann, J. D. Urbina, and M. R. Dennis, Phys. Rev. E **79**, 016203 (2009).
[31] H. Ishio and J. P. Keating, J. Phys. A **37**, L217 (2004).
[32] D. S. Fisher and P. A. Lee, Phys. Rev. B **23**, 6851 (1981).
[33] R. Landauer, Zeitschrift für Physik B: Condensed Matter **68**, 217 (1987).
[34] R. Landauer, IBM J. Res. Develop. **1**, 233 (1957).
[35] J. B. Keller, J. Opt. Soc. Am **52**, 116 (1962).
[36] R. Kouyoumjian and P. H. Pathak, Proc. IEEE **62**, 1448 (1974).
[37] M. Sieber, N. Pavloff, and C. Schmit, Phys. Rev. E **55**, 2279 (1997).
[38] S. Rotter, B. Weingartner, F. Libisch, F. Aigner, J. Feist, and J. Burgdörfer, in *Large-Scale Scientific Computing*, Lecture Notes in Computer Science, edited by I. Lirkov, S. Margenov, and J. Waniewski, Vol. 3743 (Springer, Berlin, 2006) pp. 586–593.
[39] S. Rotter, J.-Z. Tang, L. Wirtz, J. Trost, and J. Burgdörfer, Phys. Rev. B **62**, 1950 (2000).
[40] F. Libisch, S. Rotter, and J. Burgdrfer, New J. Phys. **14**, 123006 (2012).
[41] T. Blomquist, H. Schanze, I. V. Zozoulenko, and H. J. Stöckmann, Phys. Rev. E **66**, 026217 (2002).
[42] H. G. Winful, Phys. Rev. Lett. **91**, 260401 (2003).
[43] G. Tanner, K. Richter, and J.-M. Rost, Rev. Mod. Phys. **72**, 497 (2000).
[44] D. Wintgen, K. Richter, and G. Tanner, Chaos **2**, 19 (1992).
[45] G. S. Ezra, K. Richter, G. Tanner, and D. Wintgen, J. Phys. B **24**, L413 (1991).
[46] U. Fano, Phys. Rev. **124**, 1866 (1961).
[47] P. Cvitanović and B. Eckhardt, Phys. Rev. Lett. **63**, 823 (1989).
[48] B. Eckhard, G. Russberg, P. Cvitanovic, P. Rosenqvist, and P. Scherer, in *Quantum chaos*, edited by G. Casati and B. Chirikov (Cambridge University Press, Cambridge, 1995) pp. 405–434.
[49] P. Gaspard and S. A. Rice, J. Chem. Phys. **90**, 2242 (1989).
[50] Y. F. Chen, K. F. Huang, and Y. P. Lan, Phys. Rev. E **66**, 046215 (2002).
[51] R. Akis, D. K. Ferry, and J. P. Bird, Phys. Rev. Lett. **79**, 123 (1997).
[52] S. Rotter, P. Ambichl, and F. Libisch, Phys. Rev. Lett. **106**, 120602 (2011).
[53] Y.-H. Kim, M. Barth, H.-J. Stöckmann, and J. P. Bird, Phys. Rev. B **65**, 165317 (2002).
[54] D. Subramaniam, F. Libisch, Y. Li, C. Pauly, V. Geringer, R. Reiter, T. Mashoff, M. Liebmann, J. Burgdörfer, C. Busse, T. Michely, R. Mazzarello, M. Pratzer, and M. Morgenstern, Phys. Rev. Lett. **108**, 046801 (2012).
[55] C. M. Marcus, R. M. Westervelt, P. F. Hopkins, and A. C. Gossard, Phys. Rev. B **48**, 2460 (1993).
[56] A. Bärnthaler, S. Rotter, F. Libisch, J. Burgdörfer, S. Gehler, U. Kuhl, and H.-J. Stöckmann, Phys. Rev. Lett. **105**, 056801 (2010).
[57] A. Puri and J. L. Birman, J. Opt. Soc. Am. A **3**, 543 (1986).
[58] J. D. Jackson, *Classical Electrodynamics*, 3rd ed. (Wiley, New York, 1998).
[59] D. Q. Chowdhury, D. H. Leach, and R. K. Chang, J. Opt. Soc. Am. A **11**, 1110 (1994).
[60] D. H. Foster, A. K. Cook, and J. U. Nöckel, Opt. Lett. **32**, 1764 (2007).
[61] J. Unterhinninghofen, J. Wiersig, and M. Hentschel, Phys. Rev. E **78**, 016201 (2008).
[62] H. Schomerus and M. Hentschel, Phys. Rev. Lett. **96**, 243903 (2006).